

Impacts of wind farms on land surface temperature

Liming Zhou¹, Yuhong Tian², Somnath Baidya Roy³, Chris Thorncroft¹, Lance F. Bosart¹, and Yuanlong Hu⁴

¹*Department of Atmospheric and Environmental Sciences, SUNY at Albany, 1400 Washington Avenue, Albany, NY 12222, USA*

²*IMSG at NOAA/NESDIS/STAR, 5200 Auth Road, Camp Springs, MD 20746, USA*

³*Department of Atmospheric Sciences, University of Illinois, 105 South Gregory Street, Urbana, IL 61801, USA*

⁴*Terra-Gen Power LLC, 11512 El Camino Real, San Diego, CA 92130, USA*

Correspondence

Liming Zhou

Department of Atmospheric and Environmental Sciences

University at Albany, State University of New York

1400 Washington Avenue, Albany, NY 12222

Tel: (518) 442-4446; Fax: (518) 442-5825

Email: lzhou@albany.edu

A. Supplementary Figures and Tables

Table S1. Seasonal means and standard deviations (in parenthesis) of NARR climatological 30 m wind speeds (m/s) in DJF and JJA for the period 2003-2011^a.

Time (UT) ^b	DJF	JJA
00:00	1.61 (0.47)	5.01 (0.42)
03:00	2.01 (0.39)	4.65 (0.34)
06:00	2.44 (0.54)	5.09 (0.33)
09:00	2.16 (0.51)	4.37 (0.54)
12:00	1.99 (0.51)	4.06 (0.48)
15:00	1.96 (0.40)	3.88 (0.66)
18:00	2.23 (0.54)	3.74 (0.63)
21:00	2.28 (0.59)	3.95 (0.54)

Note: ^aWind speeds are calculated as $\sqrt{u^2 + v^2}$, where u and v represent the two components of the wind. Monthly mean NARR winds of 30m above the surface at 32 km resolution are used to create the climatological winds in DJF and JJA. ^bThe NARR winds are provided at Universal Time (UT). The values at 06:00 and 18:00 UT are chosen to represent the winds at nighttime (local midnight, in black) and daytime (local noon, in gray) data, which roughly correspond to the MODIS measurement times.

Table S2. Linear trends and 95% confidence intervals (in parenthesis)^a.

Variable	Daytime	Nighttime	
DJF LST (°C)	0.233 (0.494)	0.458 (0.210)	Figures 3a and 3b
JJA LST (°C)	-0.037 (1.500)	0.724 (0.423)	Figures 3a and 3b
DJF Albedo	0.013 (0.010)	-	Figure 3c
JJA Albedo	0.007 (0.010)	-	Figure 3c

Note: ^aLinear trends (/10yrs) and the 95% confidence intervals (/10yrs) are estimated using least squares fitting.

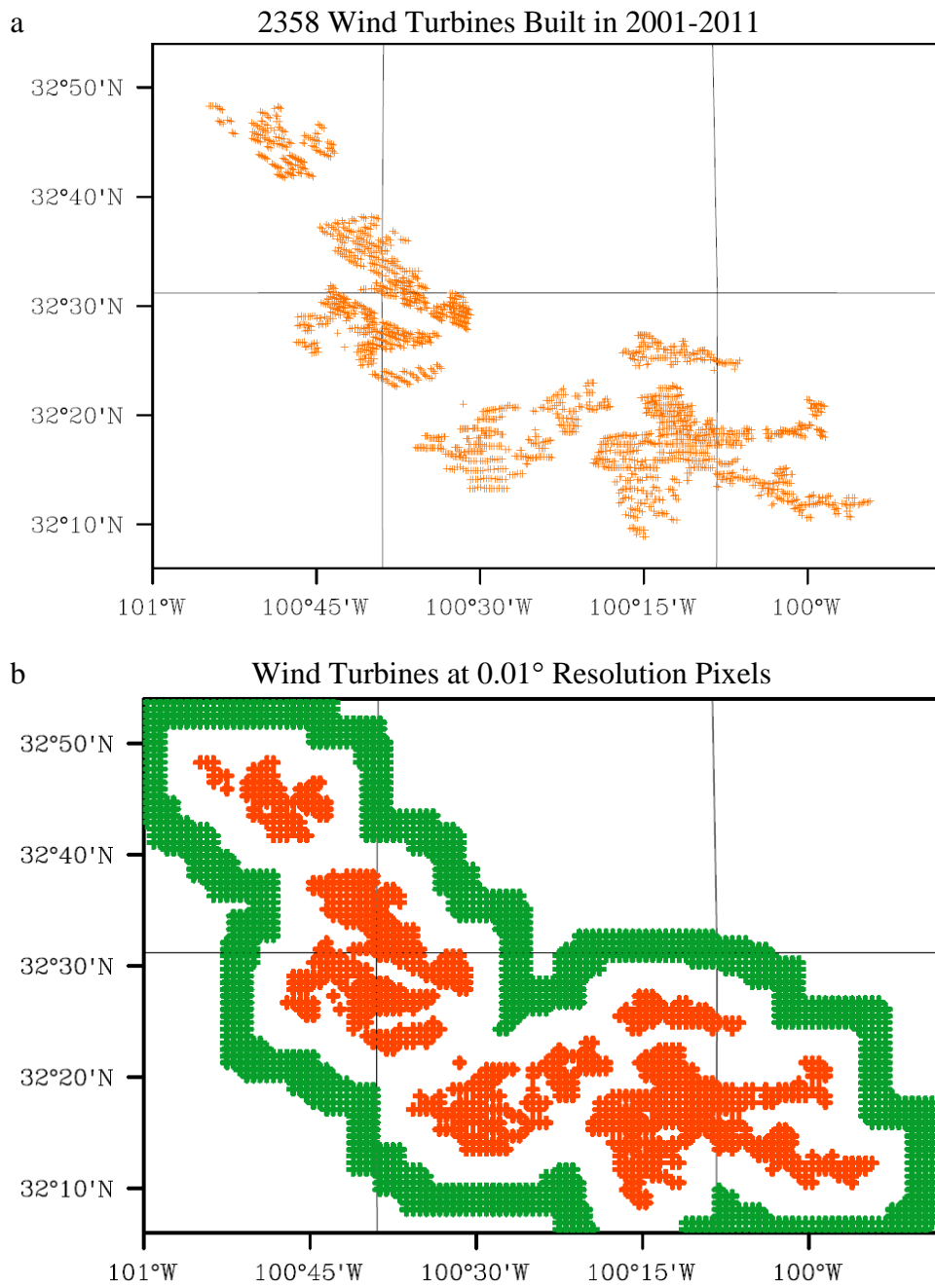


Fig. S1. 2358 individual wind turbines built in the period 2001-2011 based on the data from FAA: (a) geographic locations (latitude and longitude) of the turbine sites (the plus symbol in red) and (b) corresponding pixels at 0.01° resolution. Pixels with at least one wind turbine are defined as Wind Farm (WFM) pixels (in total: 890 pixels in red), and those that are between 6 to 9 pixels (4 pixels in width) away from the WFM pixels are defined as Nearby-Non-Wind-Farm (NNWF) pixels (in total: 1538 pixels in green). The pixels between the WFM and NNWF pixels (about 5 pixels between red and green pixels) are defined as the transition zone given the difficulty in objectively defining the boundary of downwind impacts of wind farms. Note that these wind turbines can be seen via Google Earth.

Histograms of Wind Turbines Built Annually

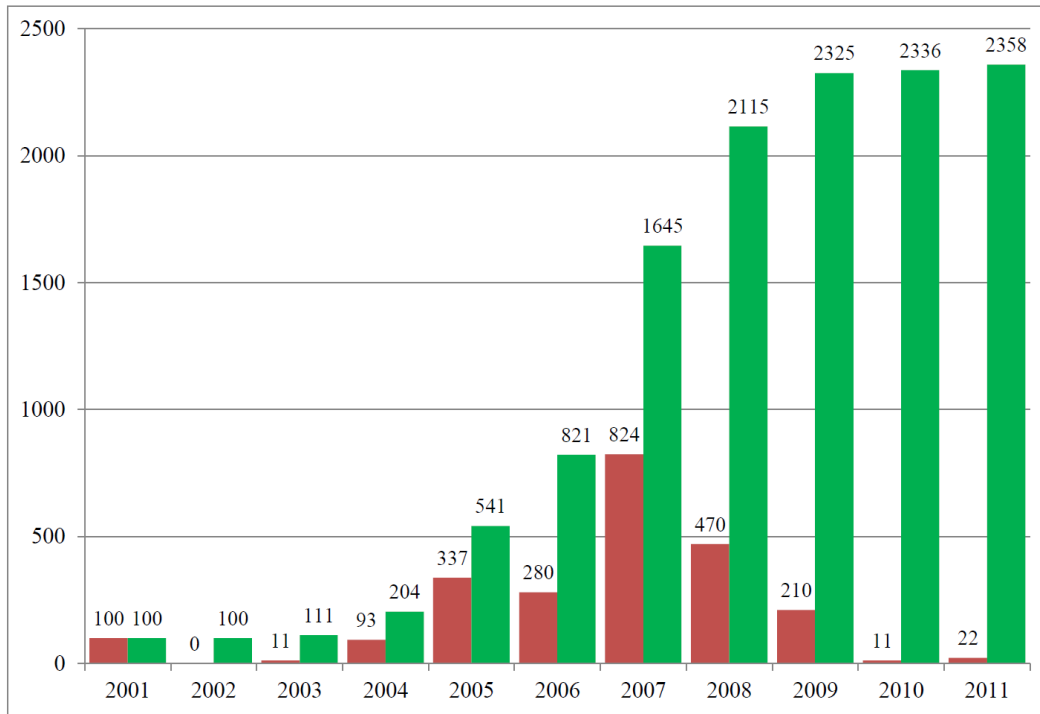


Fig. S2. Histograms of individual wind turbines built annually for the period 2001-2011 based on the FAA record. The number of annual (red) and accumulated (green) turbines built for each year is listed on the top of each bar.

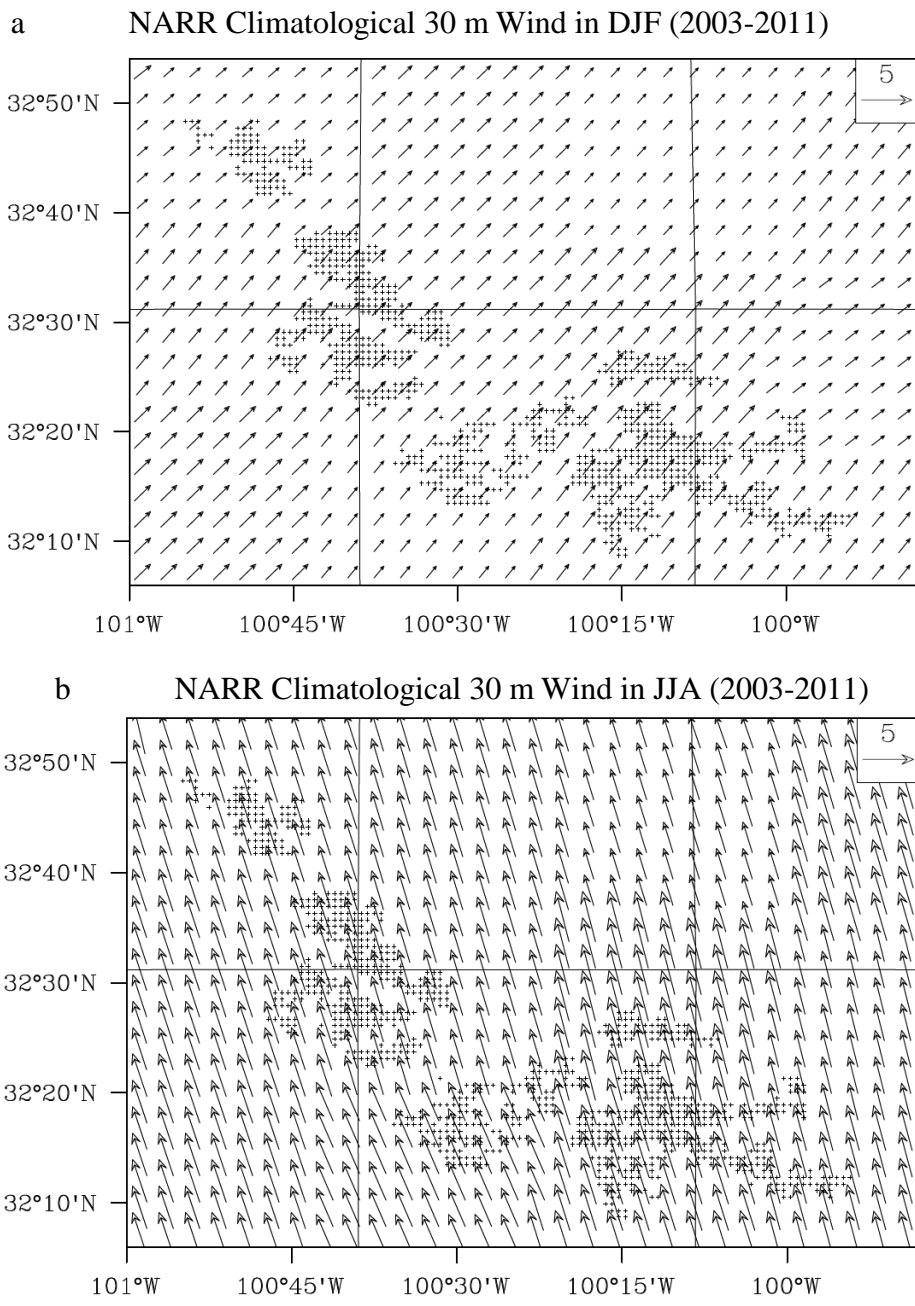


Fig. S3. NARR climatological 30 m winds (m/s) in (a) DJF and (b) JJA for the period 2003-2011. Monthly mean winds of NARR at 32 km resolution are interpolated into the 0.01° resolution pixels using bilinear interpolation and are used to create the climatological winds DJF and JJA. Pixels with plus symbol have at least one wind turbine.

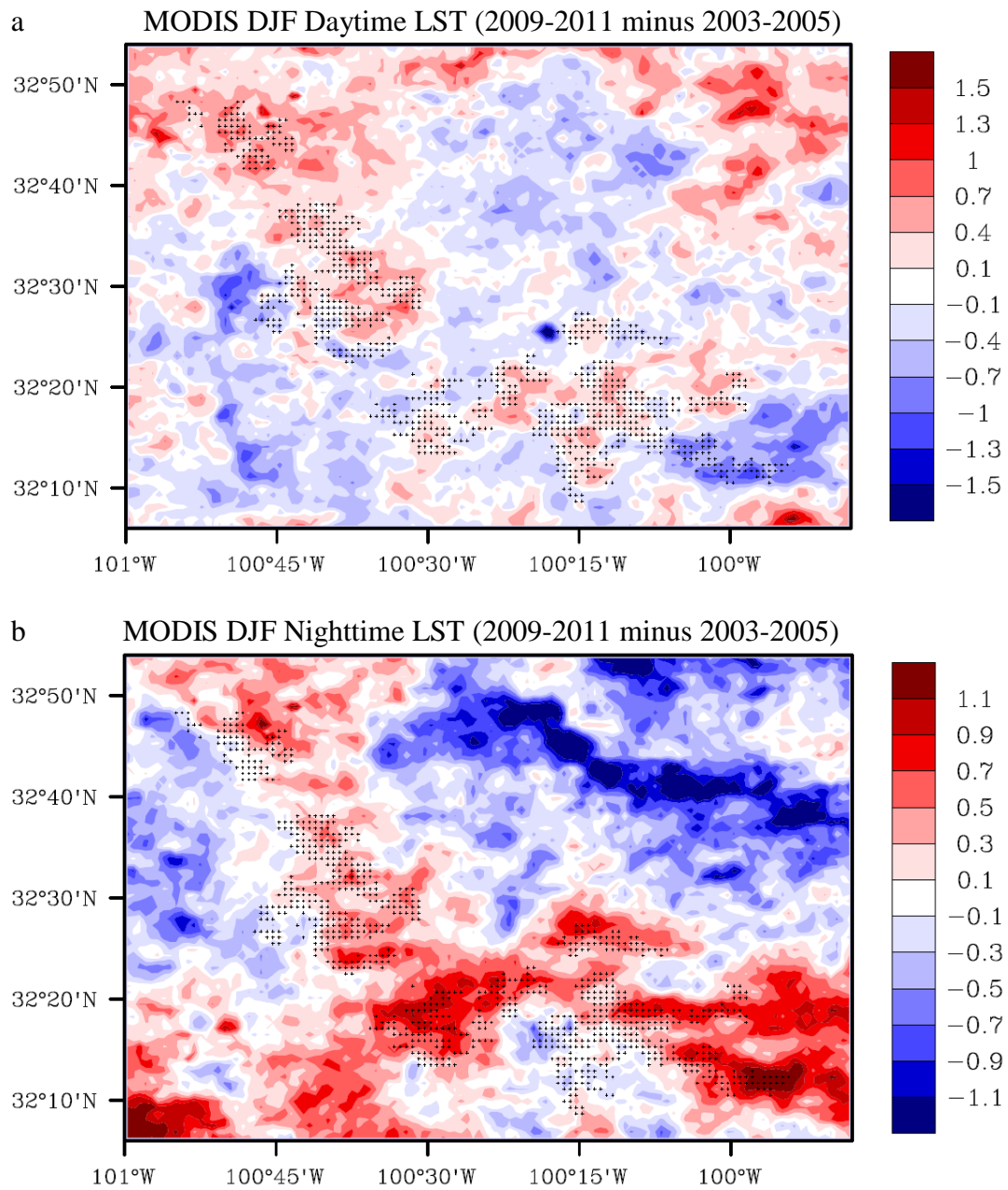


Fig. S4. MODIS DJF LST differences ($^{\circ}\text{C}$) (2009-2011 minus 2003-2005 averages) at (a) daytime and (b) nighttime. MODIS Terra and Aqua data are combined to produce daytime (averages of local solar time $\sim 10:30$ and $\sim 13:30$) and nighttime (averages of local solar time $\sim 22:30$ and $\sim 1:30$) LST. Pixels with plus symbol have at least one wind turbine. Note that the regional interannual variability was removed from the original anomalies to emphasize the relative LST changes at pixel level (i.e., Method I in the manuscript).

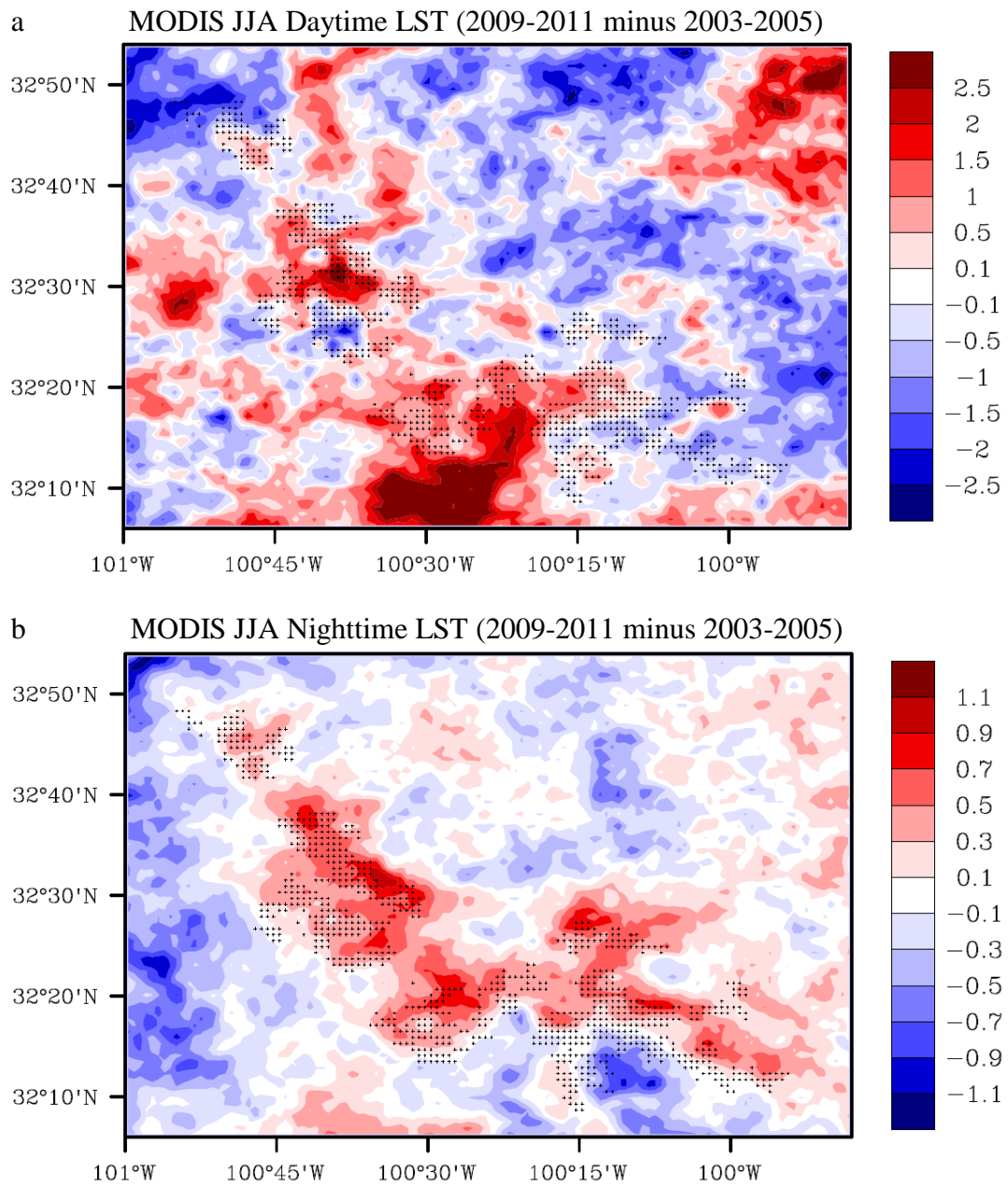


Fig. S5. MODIS JJA LST differences ($^{\circ}\text{C}$) (2009-2011 minus 2003-2005 averages) at (a) daytime and (b) nighttime. MODIS Terra and Aqua data are combined to produce daytime (averages of local solar time $\sim 10:30$ and $\sim 13:30$) and nighttime (averages of local solar time $\sim 22:30$ and $\sim 1:30$) LST. Pixels with plus symbol have at least one wind turbine. Note that the regional interannual variability was removed from the original anomalies to emphasize the relative LST changes at pixel level (i.e., Method I in the manuscript).

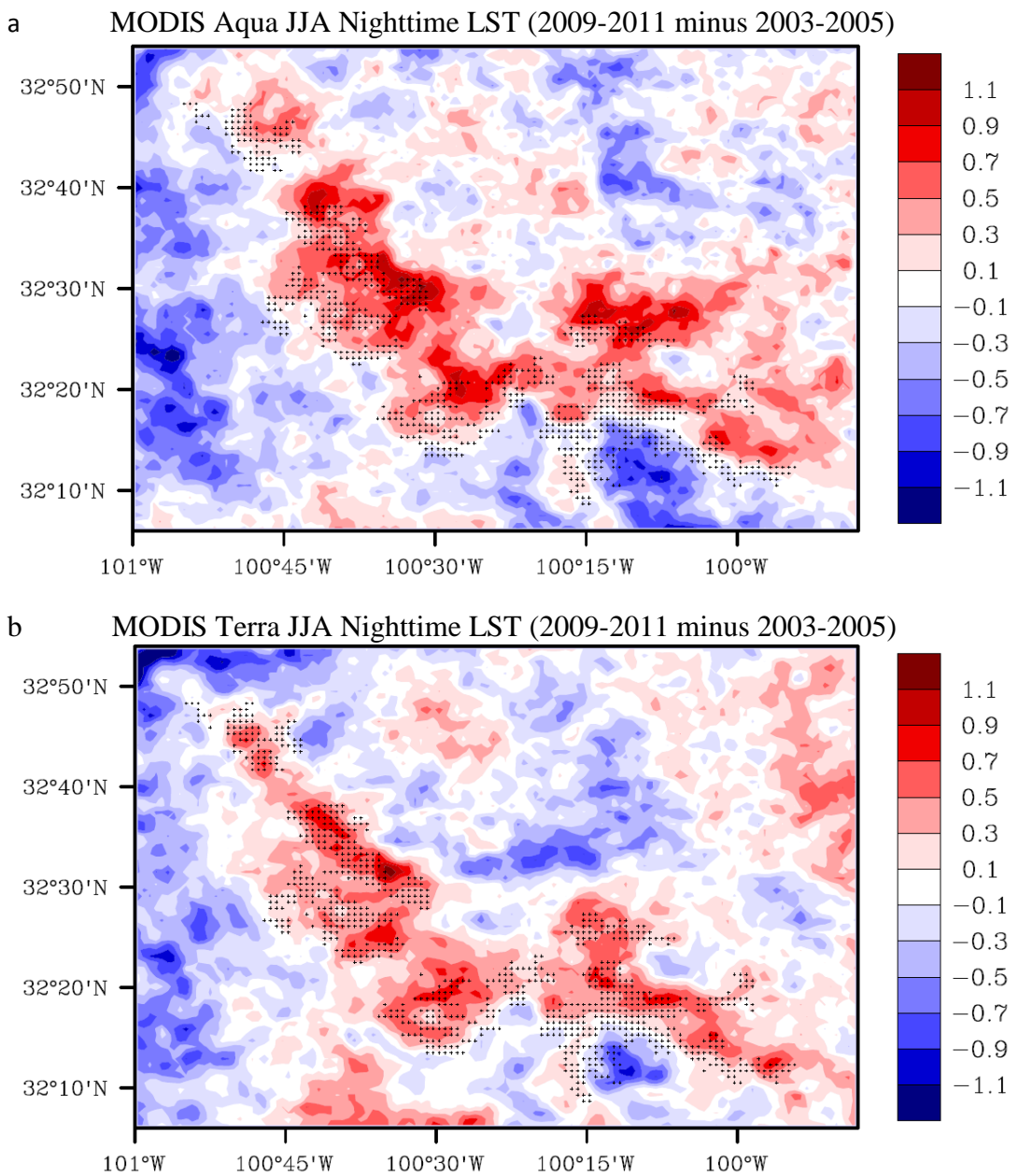


Fig. S6. MODIS JJA nighttime LST differences ($^{\circ}\text{C}$) (2009-2011 minus 2003-2005 averages) for (a) Aqua at local solar time $\sim 1:30$ and (b) Terra at local solar time $\sim 22:30$. Pixels with plus symbol have at least one wind turbine. Note that the regional interannual variability was removed from the original anomalies to emphasize the relative LST changes at pixel level (i.e., Method I in the manuscript).

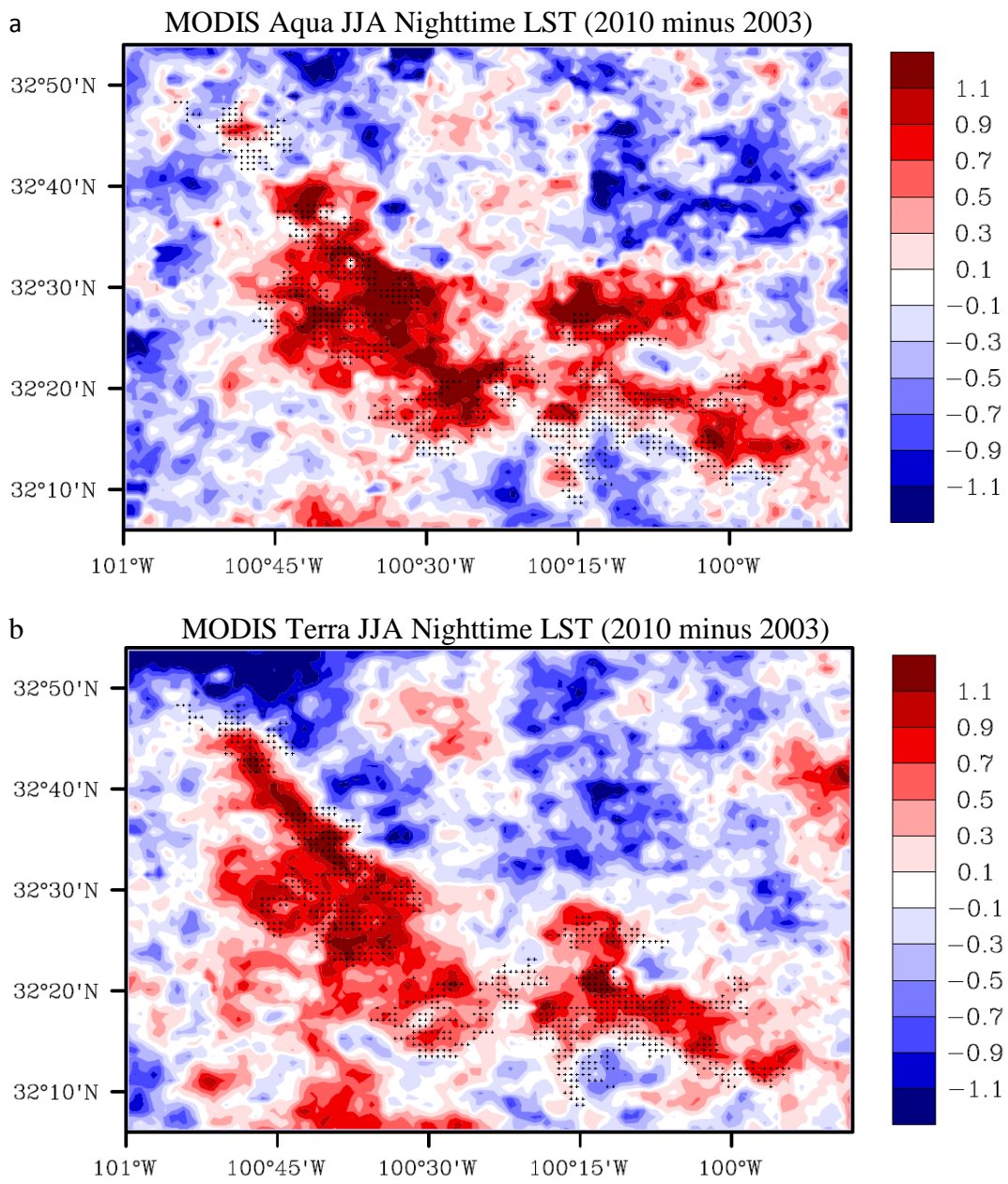


Fig. S7. MODIS JJA nighttime LST differences ($^{\circ}\text{C}$) (2010 minus 2003) for (a) Aqua at local solar time $\sim 1:30$ and (b) Terra at local solar time $\sim 22:30$. Pixels with plus symbol have at least one wind turbine. Note that the regional interannual variability was removed from the original anomalies to emphasize the relative LST changes at pixel level (i.e., Method I in the manuscript).

B. Supplementary Discussion

Assessing Impacts of Changes in Surface Elevation and Land Surface Properties on LST Variability

Here we quantify the possible impacts of spatial variations in surface elevation and land cover type and temporal variations in land surface properties on LST. Before doing so, we first provide some background information about the LST spatial-temporal variability. As the wind farm impacts are the strongest at nighttime in JJA, most of our results are shown for JJA and nighttime. For comparison purpose, all the images showing LST differences between two given periods are displayed with the same color table (and with the same scales).

B.1. LST Spatiotemporal Variability

Besides possible local impacts from wind farms, LST variability over the study region consists of two major components: (1) temporal variability controlled primarily by regional or large-scale weather and climate conditions, (2) spatial variability at pixel level controlled by spatial differences in topography and land surface properties.

For the first component, both MODIS and ERA LST exhibit strong interannual variability over the study region (e.g., Fig. 1. in the manuscript). As such variability has been discussed in the manuscript, here we focus more on the second component in the following discussion.

Fig. S8 shows the USGS elevation map (~30 m) over our study region (32.1-32.9°N, 101-99.8°W) and its surrounding areas (31.3-33.3°N, 102.1-99.1°W). Evidently, elevation varies widely over the study region and wind turbines are generally built on topographic high ground, with an average elevation of 749.10 meters and one standard deviation of 21.38 meters. There are several other wind farms near the study region, most built recently (Fig. S8a). Among these wind farms, our study region consists of four of the world's largest ones and has the highest concentration of wind turbines. Particularly, the majority of the wind turbines in the study region were built between 2005 and 2008, which makes the use of ~10 years of MODIS data possible.

Besides the variations in elevation, land cover also varies across our study region. Fig. S9 shows the climatology of albedo and vegetation greenness in JJA. Again, large spatial variability is evident. More vegetation is present in the south and east while higher albedos are observed in the north and west.

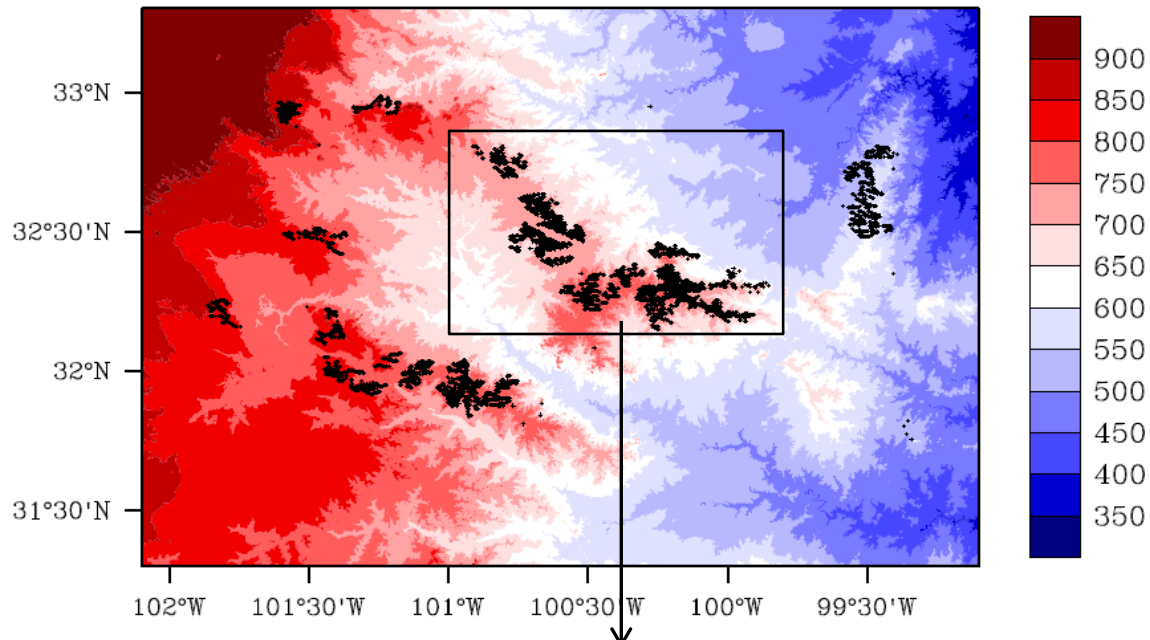
As a result, MODIS LST varies spatially (Fig. S10), mostly following the elevation and land cover patterns. The northeastern and southwestern parts of the study region are generally warmer than the southeastern and northwestern parts. The LST changes spatially, from one wind farm to another, within wind farms, and between wind farm pixels and non-wind farm pixels.

In our analysis we attempt to isolate the effect of wind farms on LST by minimizing the influence of changes in topography, land cover and regional weather/climate. Local effects at pixel level due to spatial variability in topography and land cover can be largely minimized through the use of anomalies as done in the manuscript. The strong interannual variability can be minimized by removing the regional mean LST anomaly from the original LST time series. That is why we use two methods to do so in the manuscript. Method I removes a regional mean value from the images in each year and so the LST differences between two given periods represent the

relative LST changes at pixel level (e.g., Fig.2 in the manuscript). Method II does not explicitly remove the regional mean value but implicitly performs the same function by differentiating wind farm pixels from nearby non-wind farm pixels. In other words, the use of time series anomalies at pixel level and the removal of regional interannual variability applied in the manuscript help to minimize the LST spatiotemporal variability at large scales and thus uncover the wind farm impacts.

a

USGS Elevation Map (31.3-33.3°N, 102.1-99.1°W)



b

USGS Elevation Map (32.1-32.9°N, 101-99.8°W)

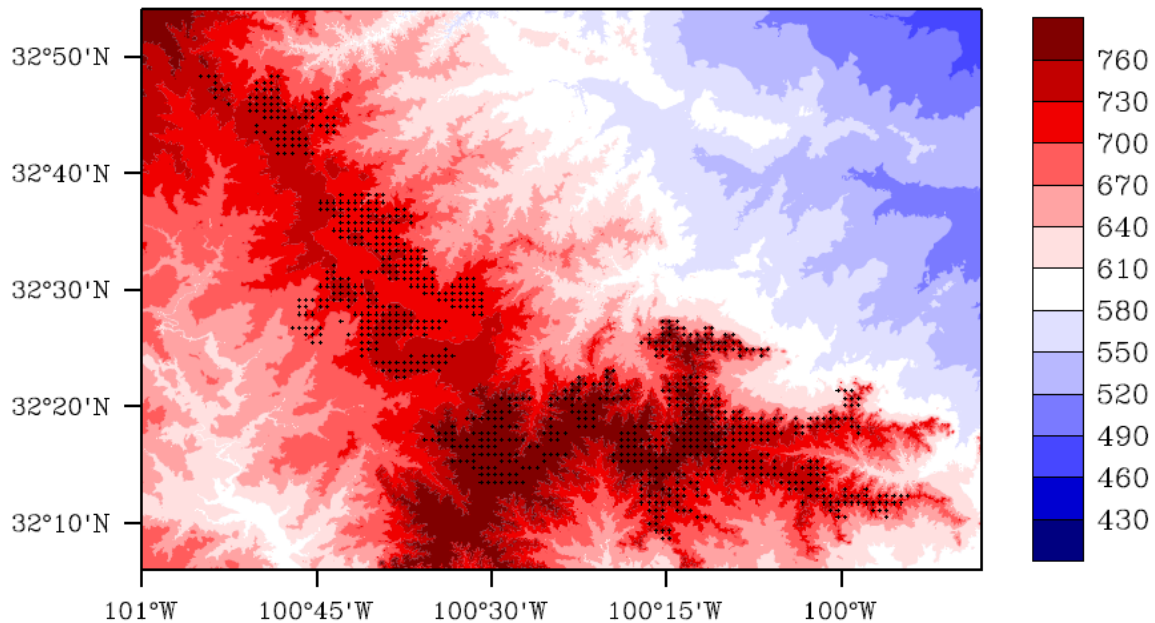
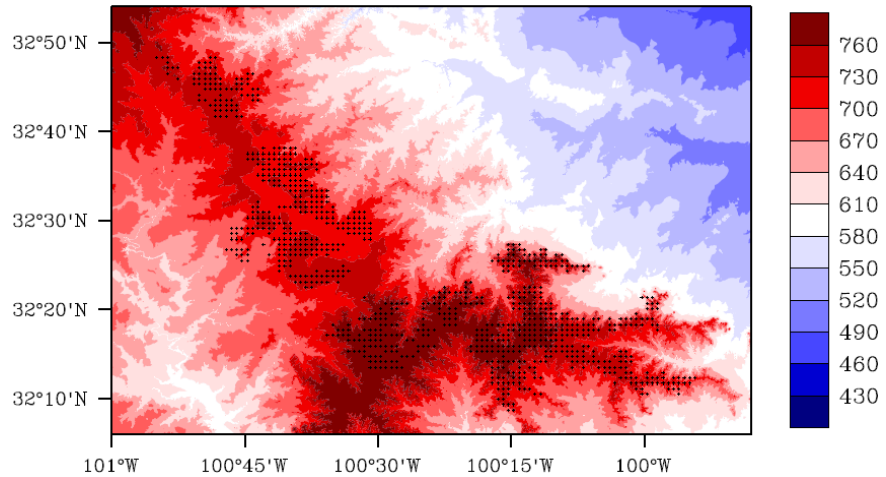
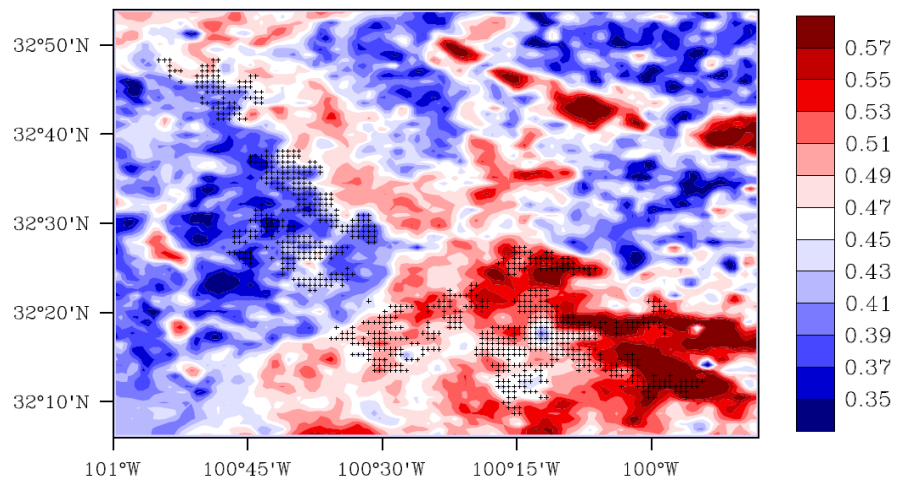


Fig. S8. USGS elevation map of our study region (32.1-32.9°N, 101-99.8°W) and its surrounding areas (31.3-33.3°N, 102.1-99.1°W) at spatial resolutions of 1 arc-second (~30 m) downloaded from <http://seamless.usgs.gov/website/seamless/viewer.htm>. Pixels with plus symbol have at least one wind turbine.

a USGS Elevation Map (32.1-32.9°N, 101-99.8°W)



b MODIS JJA NDVI Climatology (averages of 2003-2011)



c MODIS JJA Shortwave Albedo Climatology (averages of 2003-2011)

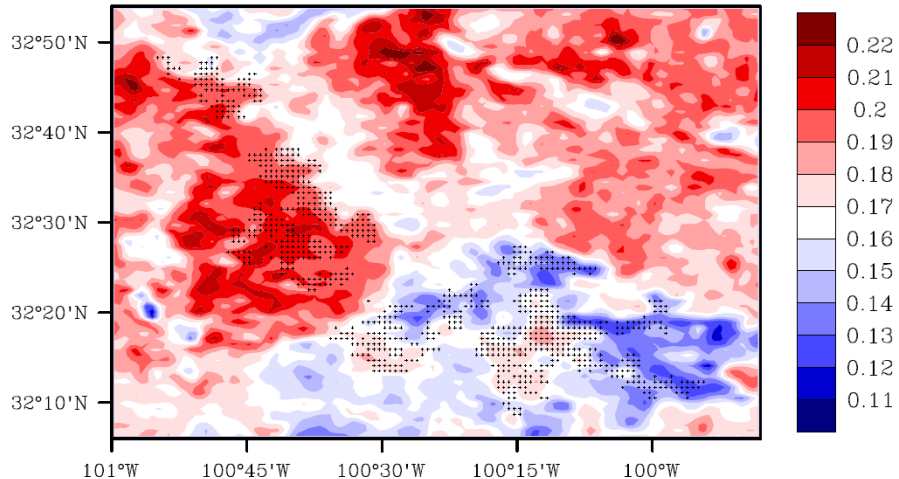
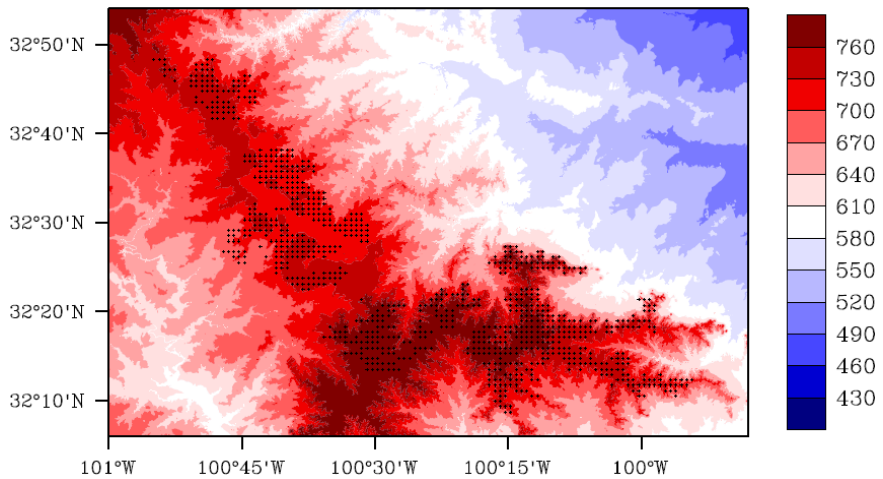
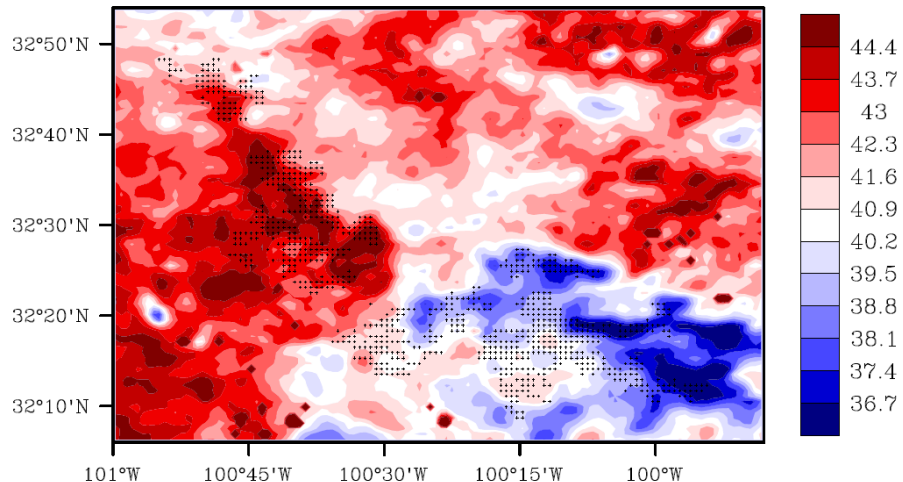


Fig. S9. (a) USGS elevation map (i.e., Fig. S8b), (b) MODIS Normalized Difference Vegetation Index (NDVI) and (c) MODIS shortwave albedo in JJA over our study region. Pixels with plus symbol have at least one wind turbine.

a USGS Elevation Map (32.1-32.9°N, 101-99.8°W)



b MODIS JJA Daytime LST Climatology (averages of 2003-2011)



c MODIS JJA Nighttime LST Climatology (averages of 2003-2011)

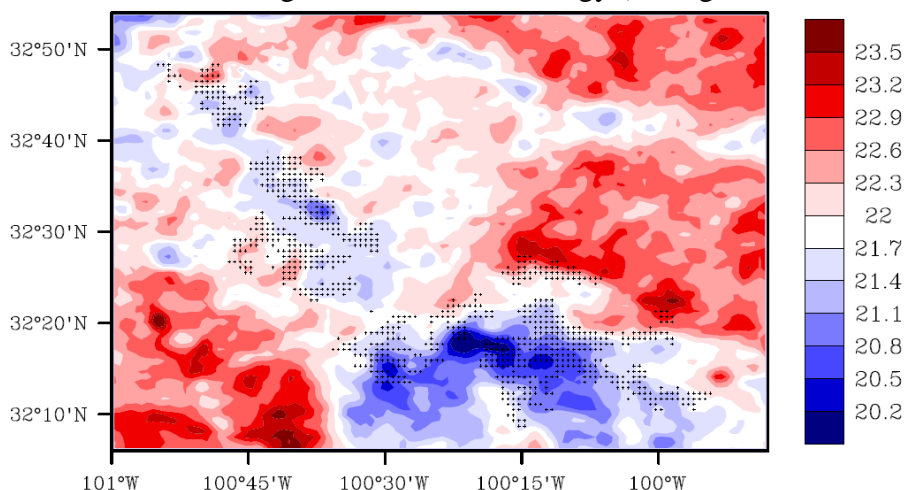


Fig. S10. (a) USGS elevation map (i.e., Fig. S8b) and climatology (averages of 2003-2011) of MODIS JJA LST at (b) daytime and (c) nighttime over our study region. Pixels with plus symbol have at least one wind turbine.

B.2. Impacts of Surface Elevation on LST Variability

Here we use three different methods to show that elevation impacts on LST are minimal and noisy while the wind farm impacts are much stronger and more consistent. The first method (Method SI) simply compares the spatial coupling between the elevation map and the warming trends shown in the manuscript. The second method (Method SII) examines how this spatial coupling evolves with time as the elevation does not change during the study period while wind farms do. The third method (Method SIII) applies the same approaches in the manuscript to a nearby control region, which has elevation patterns similar to our study region but has no built wind farms, and examines how the LST changes with elevation.

We find that all of the three methods consistently show that elevation impacts on LST are minimal and statistically insignificant.

Method SI

For this method, we simply examine the spatial coupling of surface elevations (Fig. S11a) and wind farms with the warming observed in MODIS LST (Figs. S11b and S11c, which are shown as Figs. 2a and 2b in the manuscript). If the observed warming was primarily attributable to the variations in surface elevation rather than the development of wind farms, it would couple spatially better with the former than the latter. However, the warming exhibit a stronger and more evident coupling with the wind farms than with the elevation. It is observed over most wind farm pixels but not over other high elevations without wind farms. For example, two regions (marked as A and B in Fig. S11), which have similar elevations as nearby wind farm pixels, show no warming effects while the nearby wind farm pixels do.

So it is difficult to attribute the warming trends seen by MODIS to the variations of surface elevation.

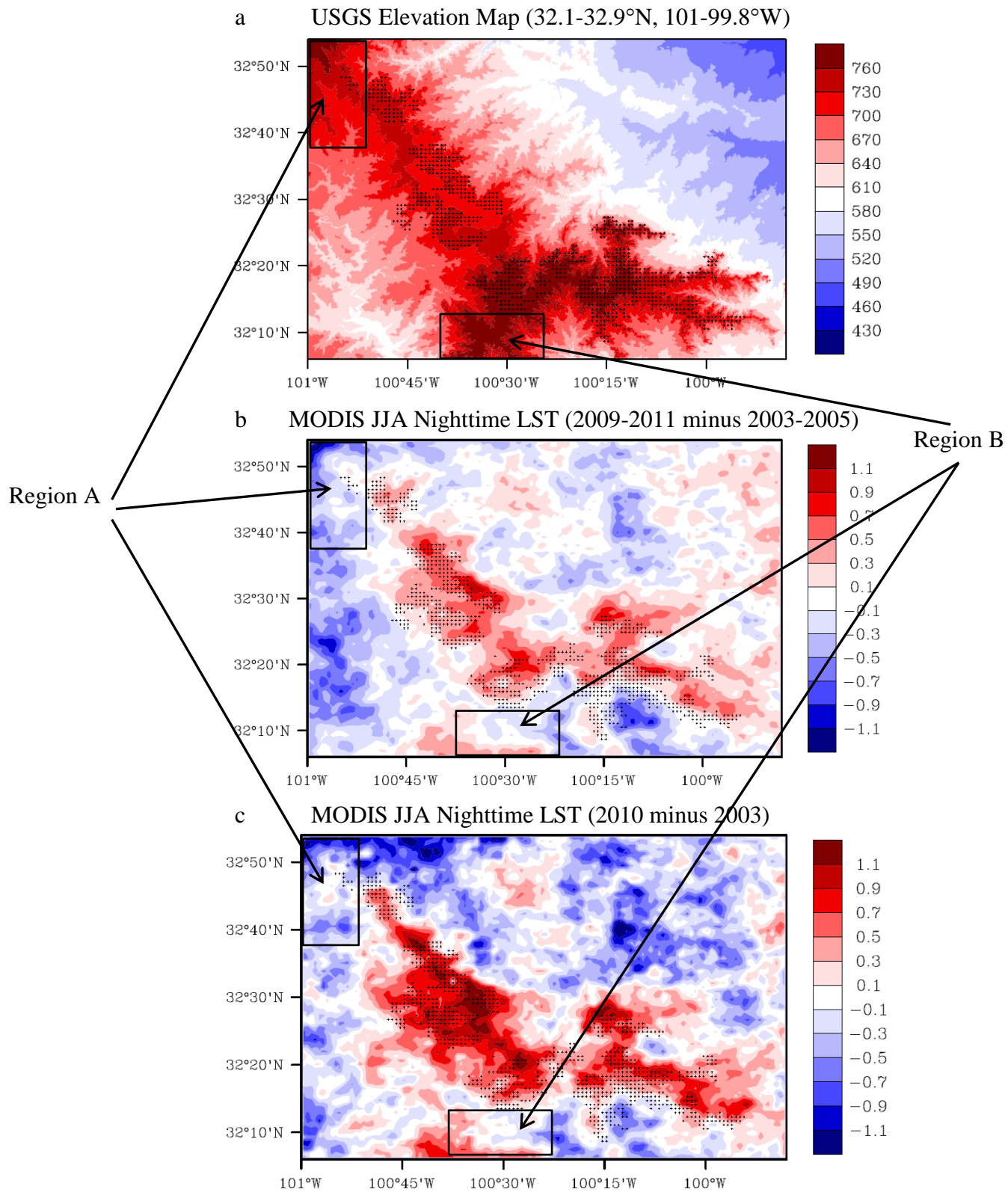


Fig. S11. (a) USGS elevation map (i.e., Fig. S8b) and MODIS JJA nighttime LST differences ($^{\circ}\text{C}$): (b) 2009-2011 minus 2003-2005 averages (i.e., Fig 2a in the manuscript) and (c) 2010 minus 2003 (i.e., Fig 2b in the manuscript), over our study region. Pixels with plus symbol have at least one wind turbine. Note that the regional interannual variability was removed in Figs. S11b-c from the original anomalies to emphasize the relative LST changes at pixel level (i.e., Method I in the manuscript).

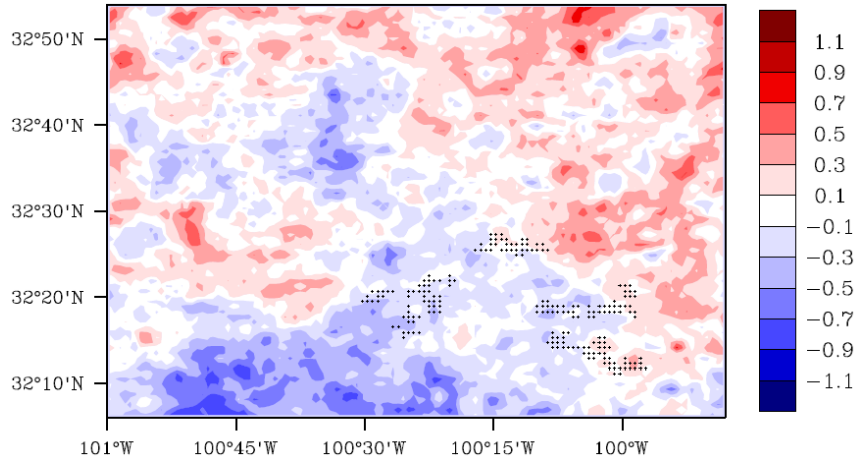
Method SII

For this method, we examine how the spatial coupling of surface elevations (Fig. S8b or Fig. S11a) and wind farms with the warming seen in MODIS LST (Figs. S12) evolves with time as the elevation does not change from 2003 to 2011 while wind farms do. Like Method SI, if the warming trend is primarily driven by the development of wind farms, we would expect to see the spatial coupling enhanced with the presence of more built wind farms.

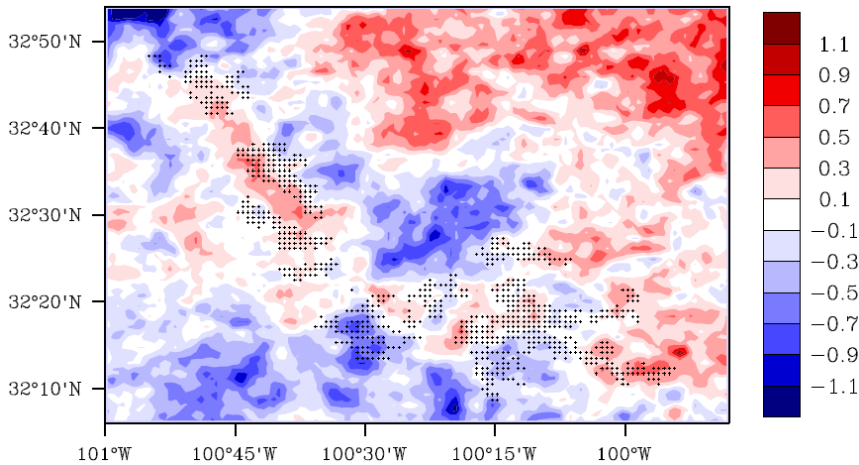
Here we use MODIS LST data for the period of 2000-2011 from Terra, which has data starting in March 2000 while Aqua has data starting in July 2002. Note that the LST data in the manuscript is created by combining both Terra and Aqua for the period 2003-2011 to reduce the LST noise and uncertainties. Although the LST from Terra alone may be slightly noisy, the additional 3 more years of MODIS Terra LST in 2000, 2001 and 2002 are very useful as this period has the least impacts of wind farms. Fig. S12 shows the JJA nighttime LST differences between the averages of 2000-2002 and those of three individual periods: 2003-2005, 2006-2008 and 2009-2011 over the study region. As expected, we do see the increasing extent and magnitude of the spatial coupling with time between the warming and the wind farms, while such coupling with elevation does not change much with time.

So it is difficult to attribute the warming trends seen by Terra to some large scale trends in static stability interacting with the varying surface topography.

a Terra JJA Nighttime LST (2003-2005 minus 2000-2002 averages)



b Terra JJA Nighttime LST (2006-2008 minus 2000-2002 averages)



c Terra JJA Nighttime LST (2009-2011 minus 2000-2002 averages)

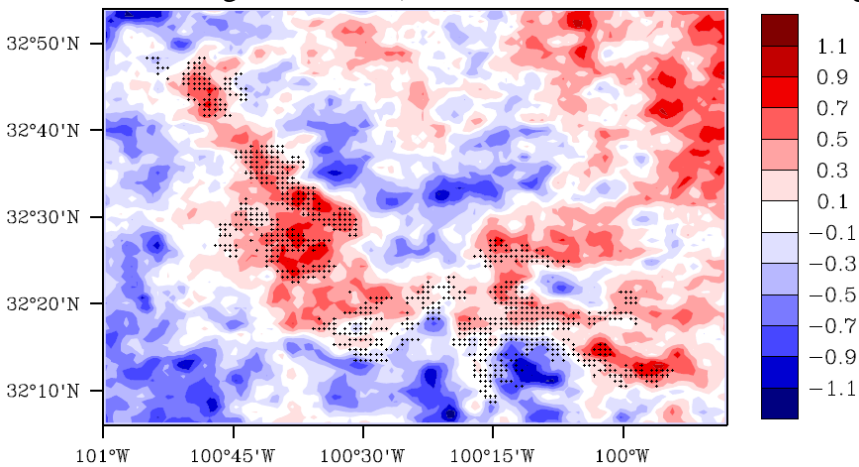


Fig. S12. Terra JJA Nighttime LST differences ($^{\circ}\text{C}$): (a) 2003-2005 minus 2000-2002 averages, (b) 2006-2008 minus 2000-2002 averages, and (c) 2009-2011 minus 2000-2002 averages, over our study region. Pixels with plus symbol have at least one wind turbine. Only those wind turbines built during each corresponding period are shown. Note that the regional interannual variability was removed from the original anomalies to emphasize the relative LST changes at pixel level (i.e., Method I in the manuscript).

Method SIII

For this method, we follow exactly what we do in the manuscript but apply our approach to another nearby region where no wind farms have been constructed. We choose an area (31.3-31.8°N, 101.2-100.2°W, referred to as our test region) to the southwest of our study region (32.1-32.9°N, 101 -99.8°W) in the manuscript (Fig. S13). The test region has similar features in terms of elevations and directions of hills and mountains as those in our study region. MODIS Terra and Aqua data are combined to produce daytime and nighttime LST as done in the manuscript. Monthly means of ERA LST at 0.75° grid boxes are also processed similarly.

First, we need to define some pixels as “wind farms” following major features of real wind farms in our study region. As most wind farms are located on topographic high ground, we use the elevation to define two regions (A with an elevation >720 meters and B with an elevation >700 meters) around the center of our test region as “wind farms” pixels. We also use the same approach as done in the manuscript to define “nearby-non-wind-farms” pixels. To differentiate these fake wind farms with real ones, we refer these pixels to as artificial wind farms (AWFM) and artificial nearby non wind farms (ANNWF) pixels. In total, there are 632 AWFM pixels and 1360 ANNWF pixels (Fig. S14).

Fig. S15 shows the regional mean LST from MODIS and ERA over our test region. Evidently, the LST exhibits strong interannual variability over the region and the variability of MODIS matches very well with that of ERA. Also, our test region exhibits similarities in terms of the interannual variability with our study region (i.e., Fig.1 in the manuscript). For example, both regions have the warmest year in 2011 and the coldest year in 2007. So overall, our test region and our study region share similar weather and climate conditions.

Again, following the approach in the manuscript, we first study the spatial patterns of LST changes and their spatial coupling with artificial wind farms by examining the LST differences between two given periods (2009-2011 minus 2003-2005 averages) (Fig. S16). Evidently, there are no strong warming trends that couple well with the artificial wind farms.

Then we quantify the impacts of the artificial wind farms on LST by examining interannual variations of areal mean JJA LST differences between AWFM versus ANNWF pixels from 2003 to 2011 (AWFM minus ANNWF, Fig. S17). There is a small increase in AWFM LST relative to ANNWF, but the linear trend: 0.18°C/10yrs ($p=0.179$) at nighttime and 0.37°C/10yrs ($p=0.668$) at daytime are small and statistically insignificant at the 5% level, while the trends for the real wind farms in our study region are much large and statistically significant at nighttime: 0.724°C/10yrs ($p=0.005$).

In summary, the elevation impacts on MODIS LST, if any, are much smaller and statistically insignificant than the strong and persistent signal of wind farm impacts.

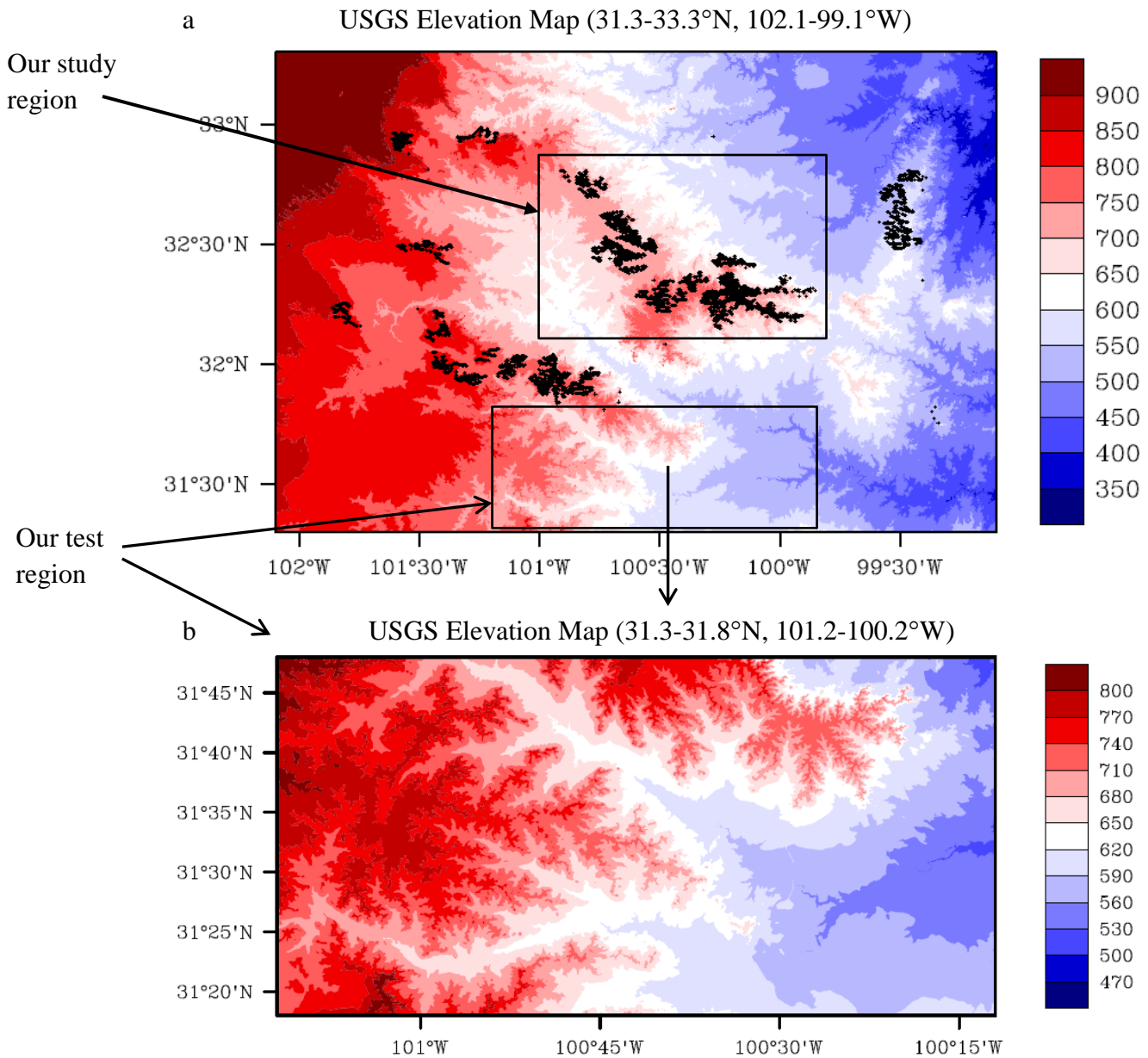


Fig. S13. (a) USGS elevation map (i.e., Fig. S8a) and (b) our test region ($31.3\text{--}31.8^\circ\text{N}$, $101.2\text{--}100.2^\circ\text{W}$).

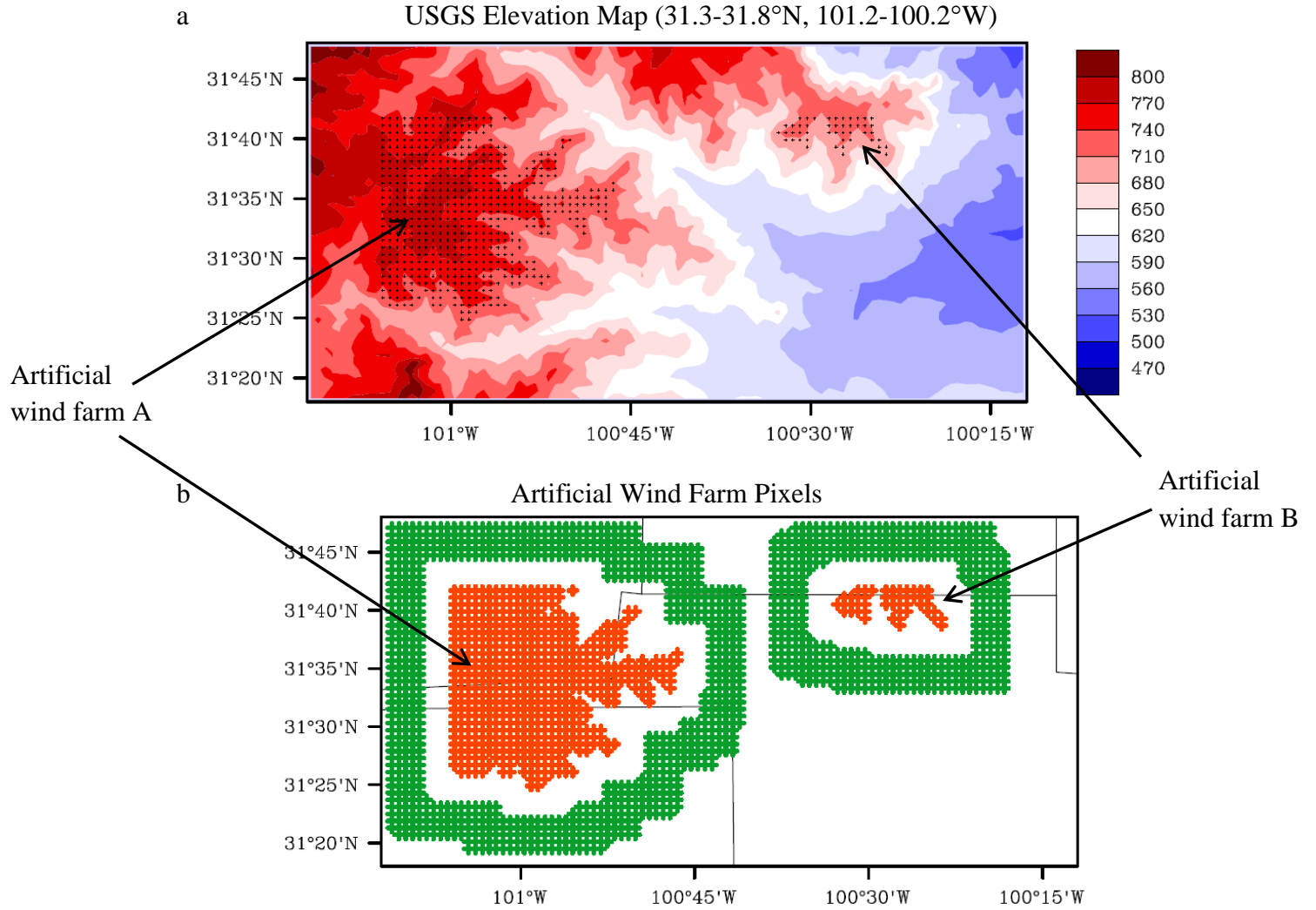


Fig. S14. (a) USGS elevation map (i.e., Fig. S13b) and (b) artificial wind farm pixels at resolution of 0.01° over our test region. We define the pixels with elevation >720 m for region A and >700 m for region B as the artificial wind farm (AWFM) pixels and those that are between 6 to 9 pixels (4 pixels in width) away from the AWFM pixels as the artificial nearby-non-wind-farm (ANNWF) pixels. We leave a transition zone of 5 pixels between the AWFM and ANNWF pixels as done in the manuscript. In total, there are 632 AWFM pixels (in red) and 1360 ANNWF pixels (in green).

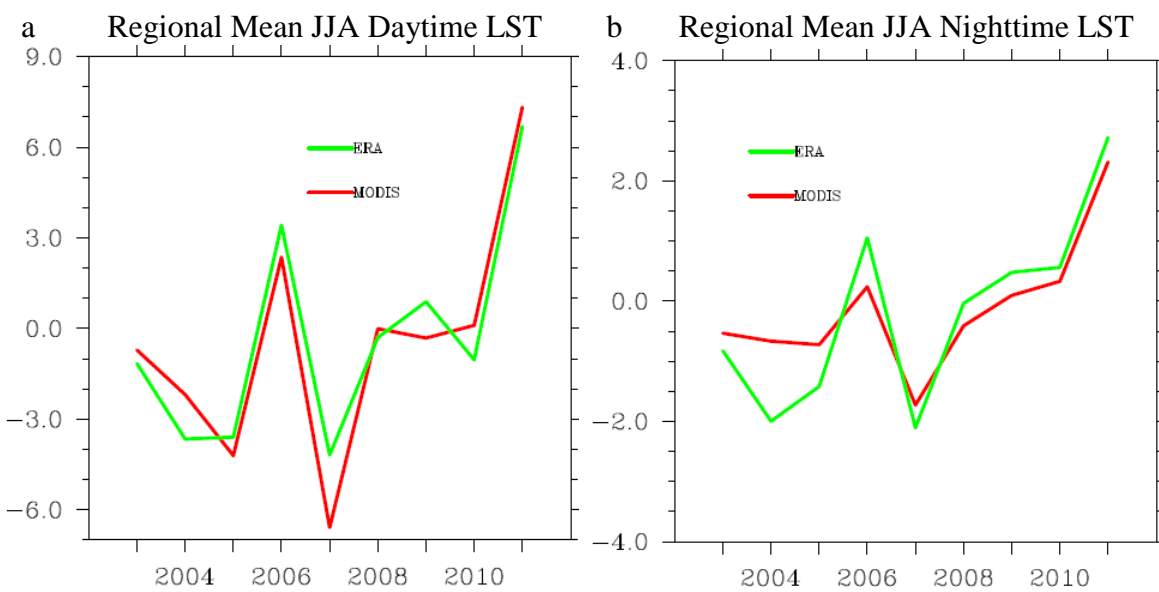


Fig. S15. Interannual variations of regional mean MODIS and ERA LST ($^{\circ}\text{C}$) anomalies in JJA at (a) daytime and (b) nighttime averaged over the test region for the period 2003-2011. MODIS and ERA are processed as done in the manuscript.

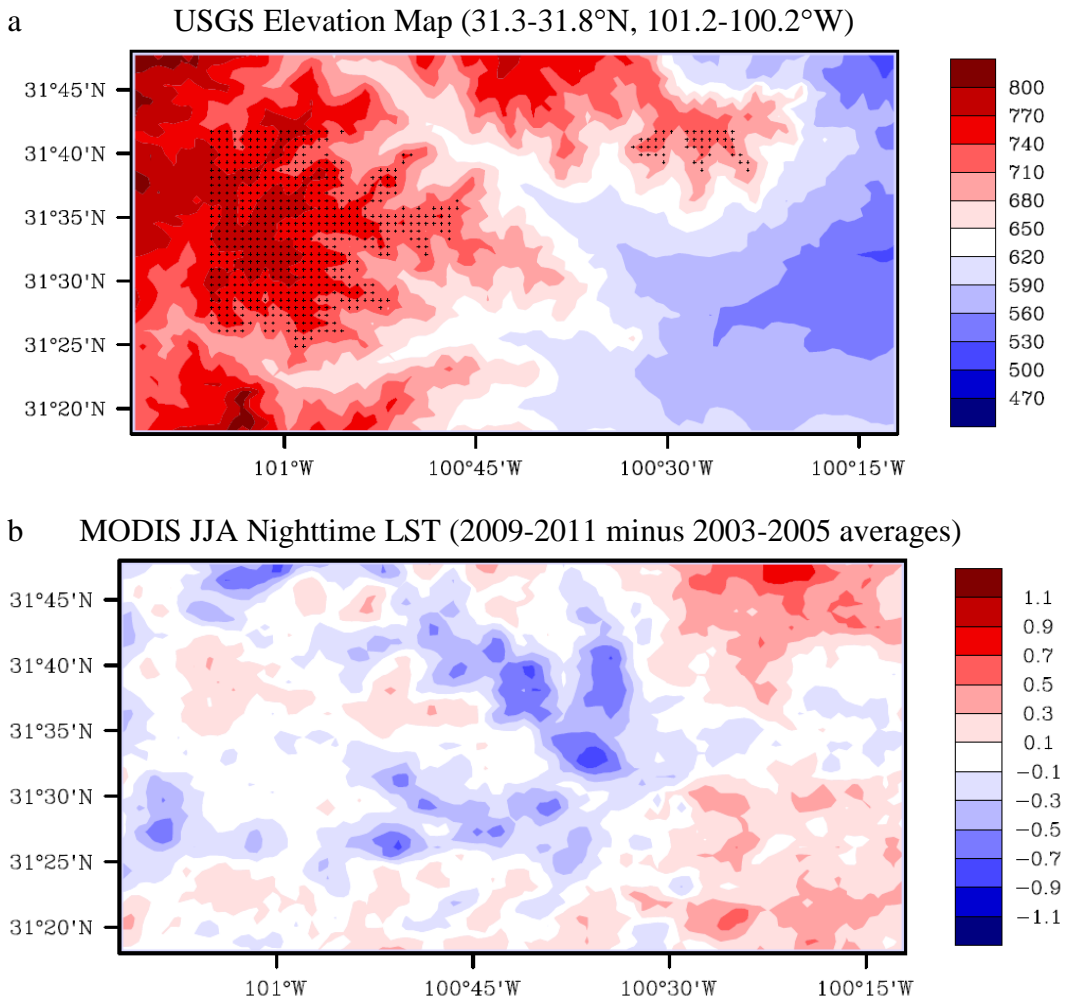


Fig. S16. (a) USGS elevation map at resolution of 0.01° (i.e., Fig. S14a) and (b) MODIS JJA nighttime LST differences ($^{\circ}\text{C}$) between 2009-2011 and 2003-2005, at resolution of 0.01° over our test region. MODIS Terra and Aqua data are combined to produce nighttime (averages of local solar time $\sim 22:30$ and $\sim 1:30$) LST. For comparison purpose, the color table in Figs. S16b remains the same as that in Figs. S11 and S12 (or Fig. 2. in the manuscript). Note that the regional interannual variability was removed in Fig. S16b, from the original anomalies to emphasize the relative LST changes at pixel level (i.e., Method I in the manuscript) as done for other similar figures.

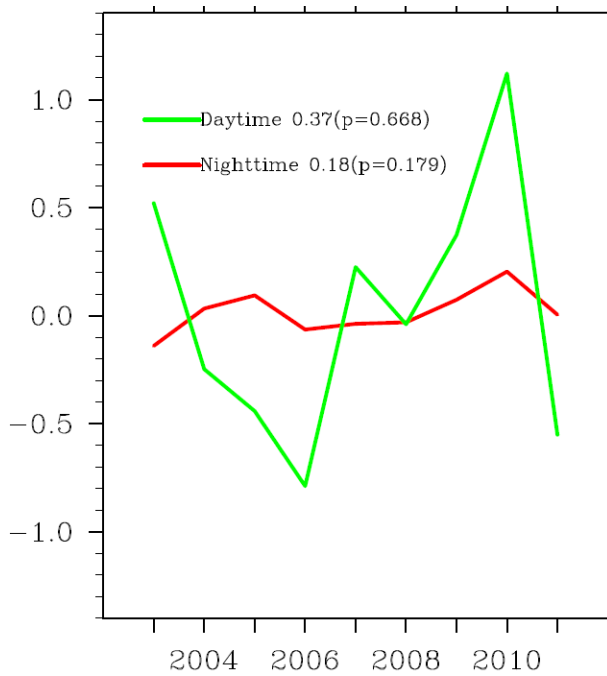


Fig. S17. Interannual variations in areal mean MODIS JJA LST ($^{\circ}\text{C}$) differences between artificial wind farm (AWFM) pixels and artificial nearby-non-wind-farm (ANNWF) pixels (AWFM minus ANNWF) for the period 2003-2011 over our test region. Linear trends ($^{\circ}\text{C}/10\text{yrs}$) and significance levels (p values) estimated using least squares fitting are shown. The 95% confidence intervals for the trends are 0.367 ± 1.936 at daytime and 0.180 ± 0.286 at nighttime, respectively. AWFM and ANNWF are defined in Fig. S14b.

B.3. Impacts of Temporal Changes in Land Surface Properties on LST Variability

Land surface properties can be also modified by temporal changes in precipitation, clouds, soil moisture, vegetation and land cover/land use (LCLU) (e.g., irrigation, agricultural practice, urbanization, etc). As there are no surface observations of these variables available at ~1.1 km, we use MODIS data of vegetation greenness, albedo and land cover to quantify possible changes in land surface properties. For example, drought will decrease soil moisture and vegetation greenness but increase surface albedo; a LCLU change from one distinct type (e.g., grasses and crops) to another (e.g., forest or urban) will cause a shift in the satellite measured reflectance spectrum and thus in land cover.

We found 10.5% (12.7%) of pixels showing LCLU changes over the ALL (WFM) pixels from 2003 to 2009. However, the changes are only between grasses/croplands and shrubs/savanna and there is no detectable change from vegetation to urban or barren lands (Table S3 and Fig. S18). Furthermore, the LULC changes exhibit no apparent WFM versus NWF differences and no spatial coupling with the LST change. We quantify changes in greenness and albedo by examining their spatial patterns and interannual variations as done for LST. On average, the mean NDVI value in 2009-2011 decreases by -0.036 (-0.051) relative to that in 2003-2005 over the ALL (WFM) pixels, while the corresponding mean albedo increases by 0.006 (0.008) (Table S4).

There is a negative spatial correlation between the albedo and greenness changes over most pixels in the study region, which is expected given their association with vegetation and soil moisture (Figs. S19-21). The overall regional mean increase (decrease) in albedo (vegetation greenness) and some large changes seen over other NWF regions (Fig.2c and Figs. S19-21) are likely due to changes in weather conditions such as the reduction in precipitation and the increase of temperature (Fig.1 and Fig. S22).

Compared to their surrounding NWF pixels, WFM pixels do show slightly larger changes, possibly related to the turbine “footprint”. For example, the linear trend of albedo is 0.007/10yrs ($p=0.149$) in JJA and 0.013/10yrs ($p=0.021$) in DJF over WFM pixels relative to NNWF pixels (Fig.3c), but such changes are too small to produce a notable daytime cooling (Figs. S4-5).

Because surface emissivity is closely related to LST, a related question is whether the emissivity change can explain the MODIS LST change. Both observations and model sensitivity studies (Zhou et al., 2003a; 2003b) show that an increase of surface albedo of 0.01 will result in a decrease of surface emissivity of 0.0015, which is too small to impact LST.

In summary, changes in land surface properties due to the turbine “footprint” and other factors cannot explain the warming effects over wind farms seen by MODIS.

Table S3. Land cover change matrix from 2003 to 2009^a

		To 2009				
		Grasses/Cereal Crops	Shrubs	Broadleaf crops	Savanna	Urban
For all pixels over the study region (9600 pixels)						
From 2003	Grasses/Cereal Crops	8397(87.469)	169(1.760)	65(0.677)	177(1.844)	0(0.000)
	Shrubs	425(4.427)	38(0.396)	1(0.010)	15(0.156)	0(0.000)
	Broadleaf crops	125(1.302)	1(0.010)	26(0.271)	0(0.000)	0(0.000)
	Savanna	33(0.344)	7(0.073)	1(0.010)	93(0.969)	0(0.000)
	Urban	0(0.000)	0(0.000)	0(0.000)	0(0.000)	27(0.281)
	Only for wind farm pixels ^b (890 pixels)					
Grasses/Cereal						
	Crops	734(82.287)	10(1.121)	4(0.448)	35(3.924)	0(0.000)
	Shrubs	48(5.493)	2(0.224)	0(0.000)	3(0.336)	0(0.000)
	Broadleaf crops	3(0.336)	0(0.000)	0(0.000)	0(0.000)	0(0.000)
	Savanna	7(0.785)	2(0.336)	0(0.000)	41(4.596)	0(0.000)
	Urban	0(0.000)	0(0.000)	0(0.000)	0(0.000)	1(0.112)

Note: ^aThe total number of pixels and their percentage (%) (in parenthesis) are listed here and the spatial patterns of those changes at pixel level are shown in Supplementary Fig. S18. The diagonal elements (in black) represent no change and the off-diagonal elements represent the land cover change from 2003 to 2009. ^bPixels having at least one wind turbine are defined as wind farm (WFM) pixels (Supplementary Fig. S1b). Among the 9600 (890) pixels over the study (WFM) region, 1017 (112) show a change in land cover, representing 10.5% (12.7%) of the total pixels for each individual regions. Note that the land cover map in 2009 is used as no MODIS land cover data is available in 2010 and 2011. However, the majority of the wind turbines were built before 2009 and so the changes detected here should be able to reflect the land cover changes related to the development of wind farms.

Table S4. Statistics in changes in surface albedo and vegetation greenness from 2003 to 2011^a

	WFM pixels ^b (890 pixels)		All pixels in the study region (9600 pixels)		
	climatology	Change magnitude	Change percentage	climatology	Change magnitude
Albedo	0.172	0.008	+4.7%	0.177	0.006
NDVI ^c	0.472	-0.051	-10.8%	0.453	-0.036

Note: ^aResults are only listed for JJA when the largest warming effect is observed; the change is calculated as the differences between the 2009-2011 and 2003-2005 averages; the climatology is calculated as the average for the period of 2003-2011. ^bPixels having at least one wind turbine are defined as wind farm (WFM) pixels (Supplementary Fig. S1b). ^cNormalized Difference Vegetation Index (NDVI) is calculated using the shortwave diffuse albedos of MODIS.

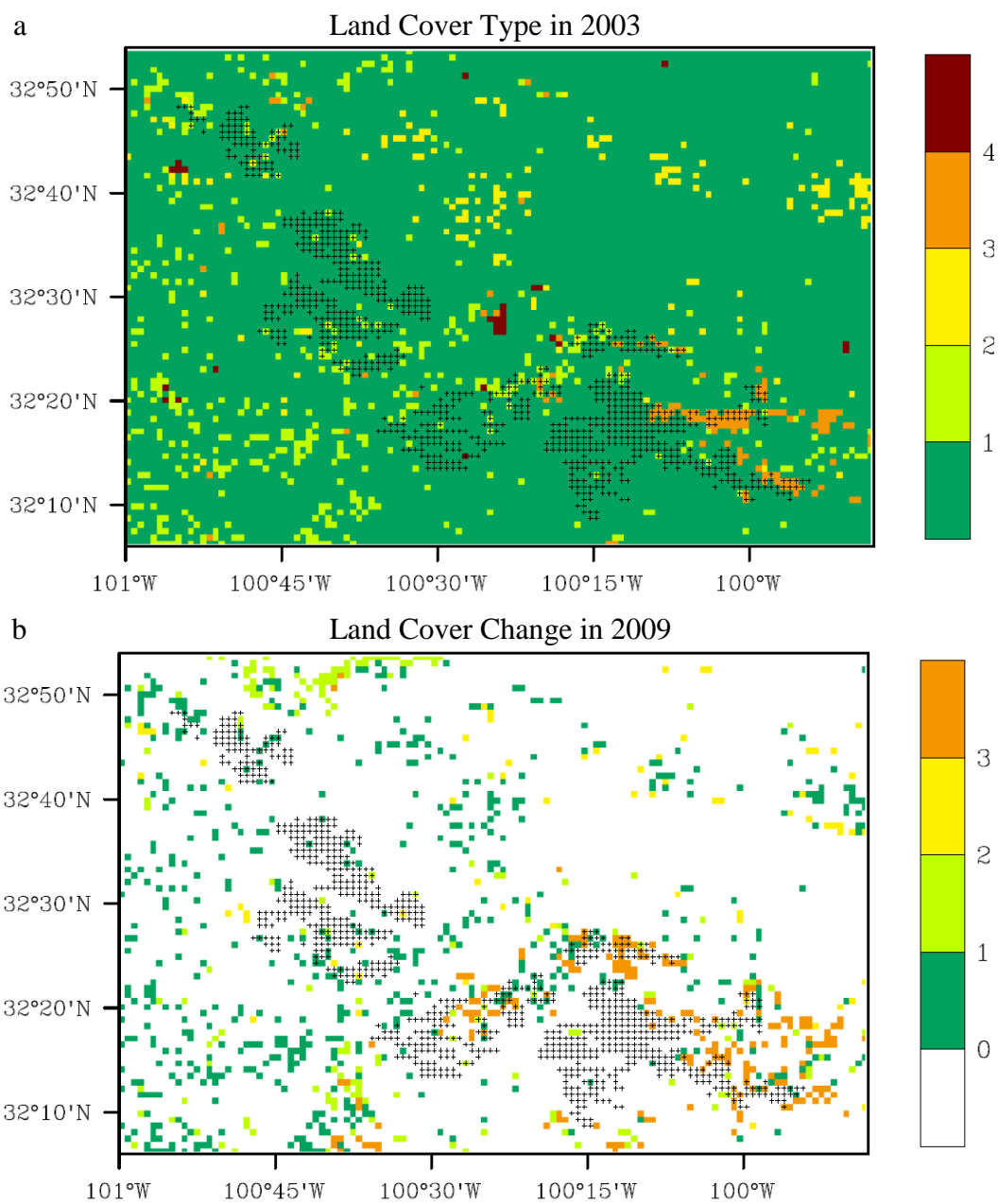


Fig. S18. MODIS land cover types in (a) 2003 and (b) their changes in 2009. There are five classes over the study region: grasses/cereal crops (1), shrubs (2), broadleaf crops (3), savanna (4) and urban (5). Figure S18b shows only those pixels whose land covers in 2009 differ from 2003 (the class type “0” represents no change). Pixels with plus symbol have at least one wind turbine and are defined as wind farm (WFM) pixels. Among the 9600 (890) pixels over the study (WFM) region, 1017 (112) show a change in land cover, representing 10.5% (12.7%) of the total pixels for each individual regions. Note that the land cover map in 2009 is used as no MODIS land cover data is available in 2010 and 2011 (see Supplementary Table S3). However, the majority of the wind turbines were built before 2009 and so the changes detected here should be able to reflect the land cover changes related to the development of wind farms.

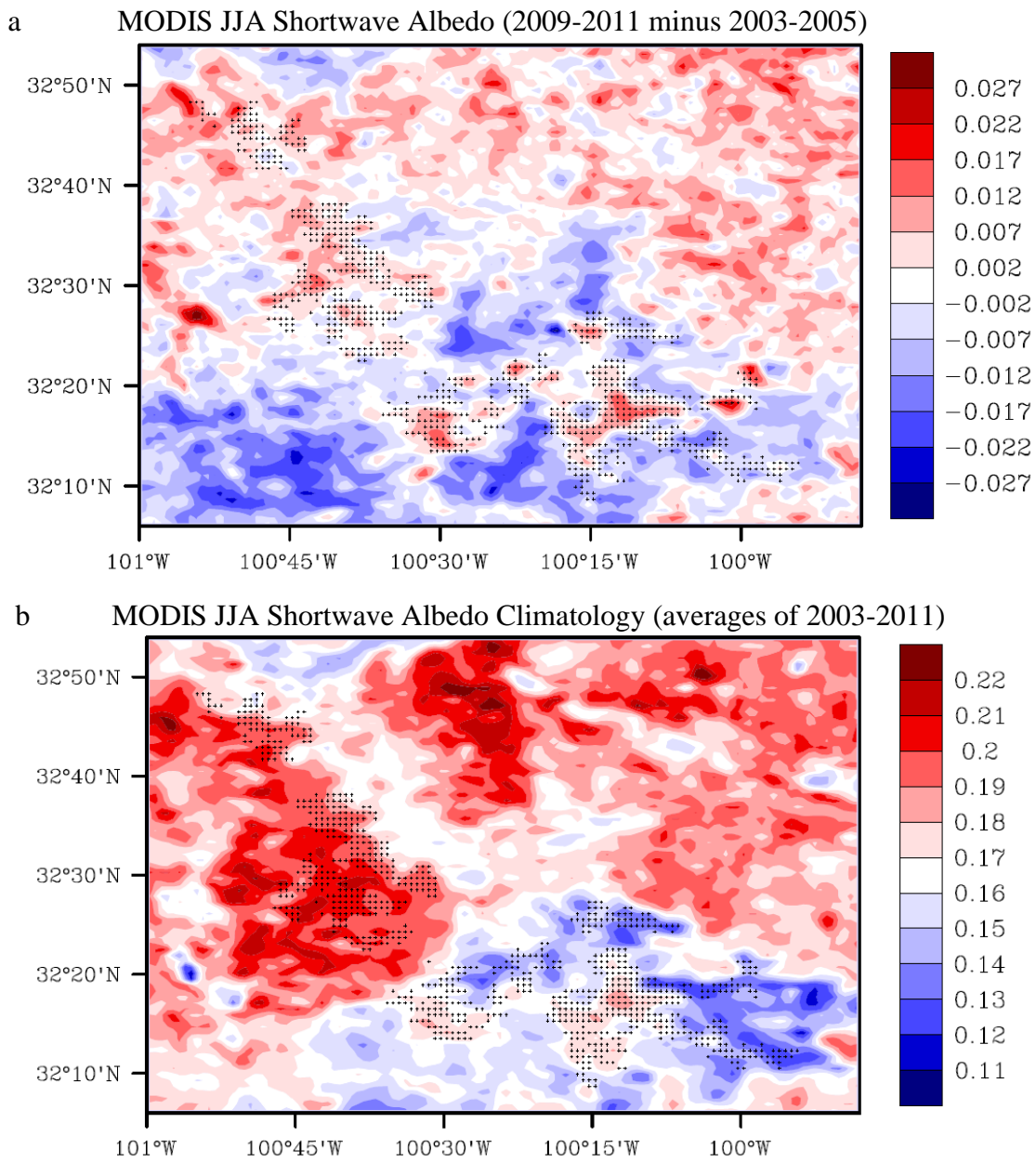


Fig. S19. MODIS shortwave albedo in JJA: (a) differences (2009-2011 minus 2003-2005 averages) and (b) the climatology for the period 2003-2011. Pixels with plus symbol have at least one wind turbine and are defined as wind farm (WFM) pixels. Note that the regional interannual variability was removed in Fig. S19a from the original anomalies to emphasize the relative albedo changes at pixel level (i.e., Method I in the manuscript). On average, the mean absolute albedo value in 2009-2011 increased by 0.006 (0.008) relative to that in 2003-2005, representing a change of 3.4% (4.7%) of the climatology value 0.177 (0.172) over the study (WFM) region (see Supplementary Table S4).

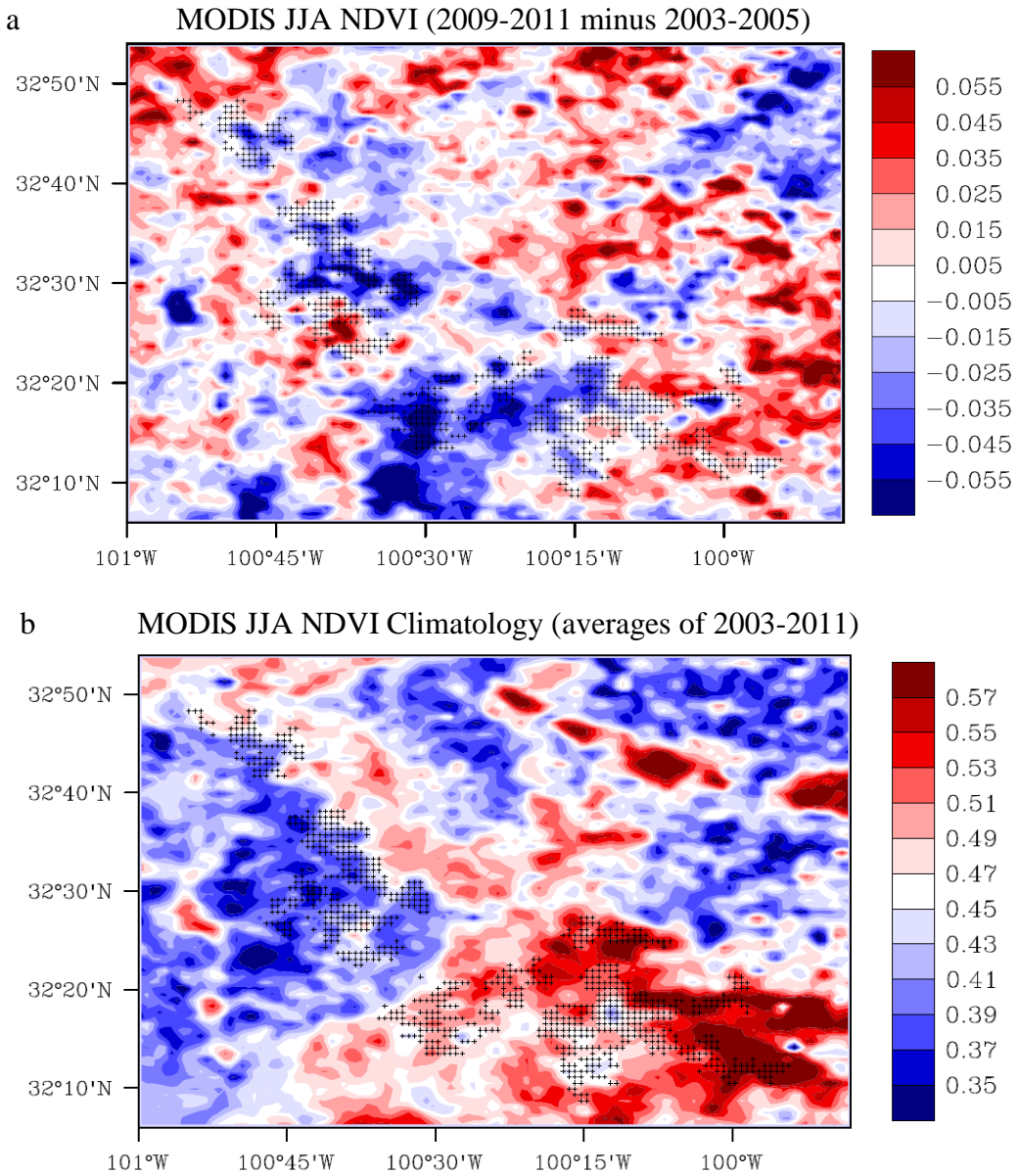


Fig. S20. MODIS Normalized Difference Vegetation Index (NDVI) in JJA: (a) differences (2009-2011 minus 2003-2005 averages) and (b) the climatology for the period 2003-2011. Pixels with plus symbol have at least one wind turbine and are defined as wind farm (WFM) pixels. Note that the regional interannual variability was removed in Fig. S20a from the original anomalies to emphasize the relative NDVI changes at pixel level (i.e., Method I in the manuscript). On average, the mean absolute NDVI value in 2009-2011 decreased by -0.0357 (-0.0512) relative to that in 2003-2005, representing a change of 7.9% (10.8%) of the climatology value 0.453 (0.472) over the study (WFM) region (see Supplementary Table S4).

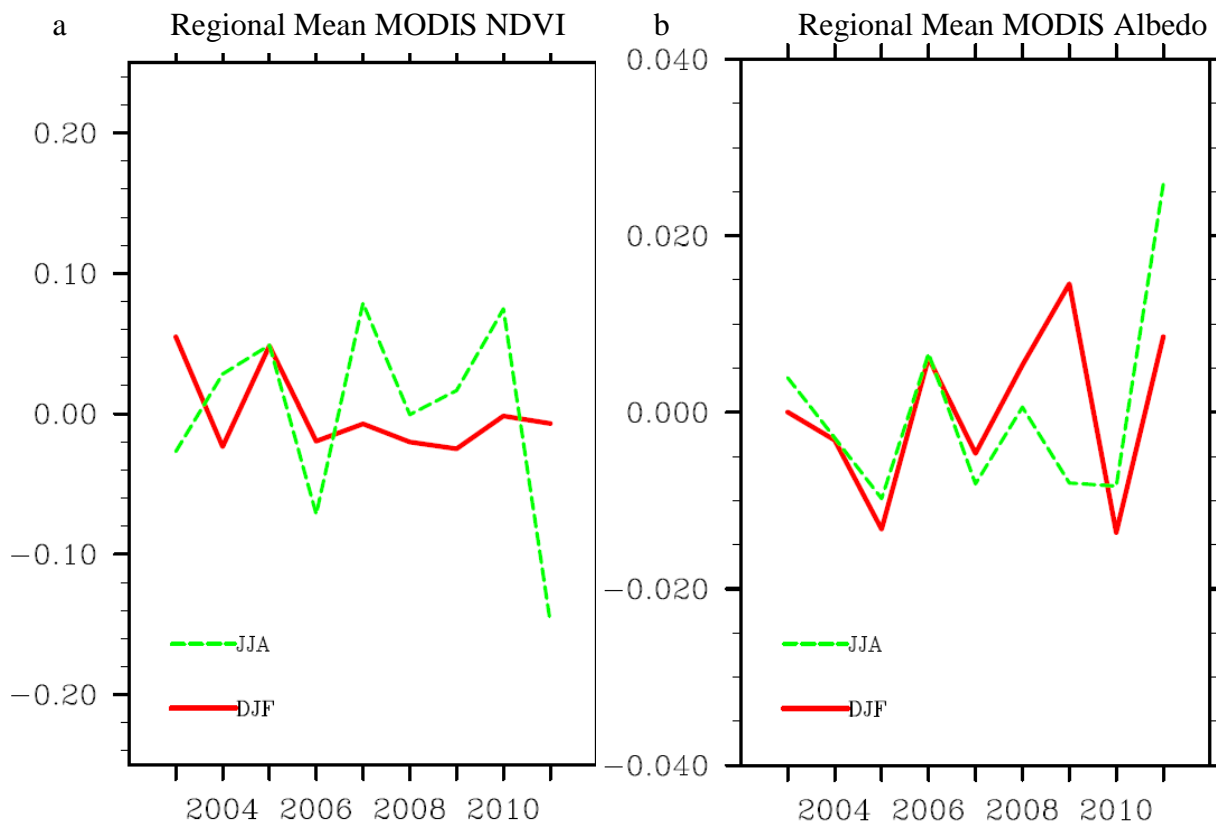


Fig. S21. Interannual variations of regional mean anomalies of (a) MODIS Normalized Difference Vegetation Index (NDVI) and (b) MODIS shortwave albedo in DJF and JJA averaged over the study region for the period 2003-2011.

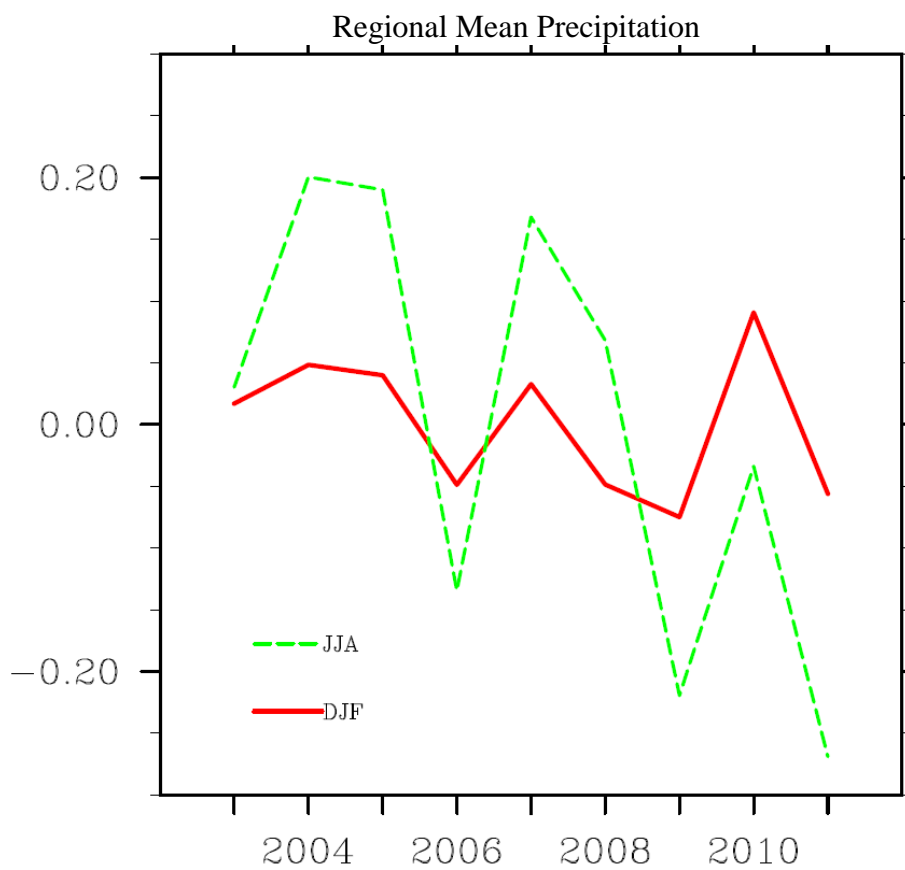


Fig. S22. Interannual variations of regional mean NARR precipitation (mm/day) anomalies in DJF and JJA averaged over the study region for the period 2003-2011. Monthly mean precipitations of NARR at 32 km resolution are interpolated into the 0.01° resolution pixels using bilinear interpolation.

References

- Zhou, L., Dickinson, R.E., Ogawa, K., Tian, Y., Jin, M., Schmugge, T., and Tsvetsinskaya, E., Relations between albedos and emissivities from MODIS and ASTER data over North African desert. *Geophys. Res. Lett.*, 30 (20), 2026, doi:10.1029/2003GL018069, 2003a.
- Zhou, L., Dickinson, R.E., Tian, Y., Jin, M., Ogawa, K., Yu, H., and Schmugge, T., A sensitivity study of climate and energy balance simulations with use of satellite derived emissivity data over the northern Africa and the Arabian peninsula. *J. Geophys. Res.*, 108(D24), 4795, doi:10.1029/2003JD004083, 2003b.